Biomedical Optics EXPRESS

Reduction of distortion in photothermal microscopy and its application to the high-resolution three-dimensional imaging of nonfluorescent tissues

Jun Miyazaki,[1,2] Hiromichi Tsurui,[3] and Takayoshi Kobayashi[1,2,4,5,*]

[1]*Advanced Ultrafast Laser Research Center, The University of Electro-Communications, 1-5-1 Chofugaoka, Chofu, Tokyo, 182-8585, Japan*
[2]*JST, CREST, K' Gobancho, 7, Gobancho, Chiyoda-ku, Tokyo 102-0076, Japan*
[3]*Department of Pathology, Juntendo University School of Medicine, 2-1-1, Hongo, Bunkyo-ku, Tokyo 113-8421, Japan*
[4]*Department of Electrophysics, National Chiao-Tung University, Hsinchu 300, Taiwan*
[5]*Institute of Laser Engineering, Osaka University, 2-6 Yamada-oka, Suita, Osaka 565-0971, Japan*
[*]*kobayashi@isl.uec.ac.jp*

Abstract: A scheme for reducing image distortion in photothermal microscopy is presented. In photothermal microscopy, the signal shape exhibits twin peaks corresponding to the focusing or defocusing of the probe beam when a sample is scanned in the axial direction. This causes a distortion when imaging a structured sample in the axial plane. Here, we demonstrate that image distortion caused by the twin peaks is effectively suppressed by providing a small offset between two the focal planes of the pump and the probe beams. Experimental results demonstrate improvement in resolution, especially in the axial direction, over conventional optical microscopy—even with the focal offset. When a dry objective lens with a numerical aperture of 0.95 is used, the full width at half the maximum of the axial point spread function is 0.6 μm, which is 50% (62%) smaller than the focal spot sizes of the pump (probe) beam. Herein, we present high-resolution three-dimensional imaging of thick biological tissues based on the present scheme.

OCIS codes: (170.6900) Three-dimensional microscopy; (350.5340) Photothermal effects.

References and links

1. E. Tamaki, K. Sato, M. Tokeshi, K. Sato, M. Aihara, and T. Kitamori, "Single-cell analysis by a scanning thermal lens microscope with a microchip: direct monitoring of cytochrome c distribution during apoptosis process," Anal. Chem. **74**(7), 1560–1564 (2002).
2. D. A. Nedosekin, E. I. Galanzha, S. Ayyadevara, R. J. Shmookler Reis, and V. P. Zharov, "Photothermal confocal spectromicroscopy of multiple cellular chromophores and fluorophores," Biophys. J. **102**(3), 672–681 (2012).
3. A. V. Brusnichkin, D. A. Nedosekin, E. I. Galanzha, Y. A. Vladimirov, E. F. Shevtsova, M. A. Proskurnin, and V. P. Zharov, "Ultrasensitive label-free photothermal imaging, spectral identification, and quantification of cytochrome c in mitochondria, live cells, and solutions," J. Biophotonics **3**(12), 791–806 (2010).
4. S. Lu, W. Min, S. Chong, G. R. Holtom, and X. S. Xie, "Label-free imaging of heme proteins with two-photon excited photothermal lens microscopy," Appl. Phys. Lett. **96**(11), 113701 (2010).
5. J. Miyazaki, H. Tsurui, K. Kawasumi, and T. Kobayashi, "Simultaneous dual-wavelength imaging of nonfluorescent tissues with 3D subdiffraction photothermal microscopy," Opt. Express **23**(3), 3647–3656 (2015).
6. C. Leduc, S. Si, J. Gautier, M. Soto-Ribeiro, B. Wehrle-Haller, A. Gautreau, G. Giannone, L. Cognet, and B. Lounis, "A highly specific gold nanoprobe for live-cell single-molecule imaging," Nano Lett. **13**(4), 1489–1494 (2013).
7. C. Leduc, J. M. Jung, R. P. Carney, F. Stellacci, and B. Lounis, "Direct investigation of intracellular presence of gold nanoparticles via photothermal heterodyne imaging," ACS Nano **5**(4), 2587–2592 (2011).
8. L. Cognet, C. Tardin, D. Boyer, D. Choquet, P. Tamarat, and B. Lounis, "Single metallic nanoparticle imaging for protein detection in cells," Proc. Natl. Acad. Sci. U.S.A. **100**(20), 11350–11355 (2003).
9. M. Selmke, M. Braun, and F. Cichos, "Photothermal single-particle microscopy: detection of a nanolens," ACS Nano **6**(3), 2741–2749 (2012).

#242711 Received 9 Jun 2015; revised 25 Jul 2015; accepted 25 Jul 2015; published 4 Aug 2015

10. M. Selmke, M. Braun, and F. Cichos, "Nano-lens diffraction around a single heated nano particle," Opt. Express **20**(7), 8055–8070 (2012).
11. K. Uchiyama, A. Hibara, H. Kimura, T. Sawada, and T. Kitamori, "Thermal lens microscope," Jpn. J. Appl. Phys. **39**(Part 1, No. 9A), 5316–5322 (2000).
12. J. Moreau and V. Loriette, "Confocal dual-beam thermal-lens microscope: Model and experimental results," Jpn. J. Appl. Phys. **45**(9A), 7141–7151 (2006).
13. J. Moreau and V. Loriette, "Confocal thermal-lens microscope," Opt. Lett. **29**(13), 1488–1490 (2004).
14. J. Miyazaki, K. Kawasumi, and T. Kobayashi, "Frequency domain approach for time-resolved pump-probe microscopy using intensity modulated laser diodes," Rev. Sci. Instrum. **85**(9), 093703 (2014).
15. J. Miyazaki, H. Tsurui, A. Hayashi-Takagi, H. Kasai, and T. Kobayashi, "Sub-diffraction resolution pump-probe microscopy with shot-noise limited sensitivity using laser diodes," Opt. Express **22**(8), 9024–9032 (2014).
16. J. Miyazaki, H. Tsurui, K. Kawasumi, and T. Kobayashi, "Sensitivity enhancement of photothermal microscopy with radially segmented balanced detection," Opt. Lett. **40**(4), 479–482 (2015).

1. Introduction

Photothermal (PT) microscopy's ability to measure light-absorbing molecules at high sensitivity and spatial resolution has made it useful in detecting endogenous non-fluorescent chromoproteins in biological tissues. Thus far, it has been applied to visualizing the distribution of cytochrome in mitochondria [1–3], the three-dimensional (3D) imaging of haemoglobin in blood vessels [4], and the high-resolution 3D imaging of melanin pigments in skin cancer [5]. Furthermore, 5-nm gold nanoparticles have been used to identify biomolecules with antibody labelling techniques that have been applied to cellular imaging by means of PT microscopy [6–8]. As gold nanoparticles are physiologically inert and do not suffer from photobleaching or photoblinking, they are useful in biological imaging and potentially applicable to immunoanalysis and gene analysis at the cellular level.

In PT microscopy, two laser beams (pump and probe) are incident on the sample through a focussing lens. The pump beam increases the temperature in the region around the light absorbing sample within the focal spot volume. This results in local refractive index changes and induces the deflection of the probe beam. In the forward detection scheme, the nano-lens (thermal lens) effect produces positive and negative peaks corresponding to the focusing or defocusing of the probe beam when a sample is scanned in the axial direction [9–11]. This signal shape would be useful in the tracking or positioning of nanomaterials, but it causes a serious problem in biological imaging, as the twin peaks result create distortion when reconstructing an image of a structured sample.

To eliminate this drawback, a confocal forward detection scheme has been proposed in previous studies [12, 13] and the experimental results have shown that a single peak with a 450-nm axial resolution is achieved when the sample is a single layer thin film and a water immersion objective lens is used. Confocal PT microscopy can be conducted with the same detection schema as the classical thermal lens setup, but the pinhole position must be carefully adjusted to avoid an unwanted photothermal signal.

In contrast, it has been demonstrated that either of the twin peaks is suppressed by an offset between the focal planes of the pump and probe beams [9]. Because the focal plane's position can be easily controlled by the divergence of the incident beam, this scheme would be a simple approach for reducing distortion without using a confocal pinhole.

The purpose of this study is to demonstrate the validity and usefulness of the offset scheme for reducing distortion in PT imaging. To this end, the relationship between the focal plane offset and the spatial resolution is examined in detail in both the lateral and axial planes, as there is concern about the degradation in the spatial resolution prompted by the focal plane offset. Experimentally, it is confirmed that both the lateral and axial resolutions are better than the convention optical microscopy, even with the offset. A procedure for reducing image distortion in PT microscopy, which has not been discussed previously, is presented and the high-fidelity 3D imaging of thick biological tissues is demonstrated.

2. Experiment

PT imaging is conducted using an LD-based pump-probe microscopic system. The details of the experimental setup and sample preparation have been described in previous papers [5, 14–

#242711 Received 9 Jun 2015; revised 25 Jul 2015; accepted 25 Jul 2015; published 4 Aug 2015

16]. A 488-nm LD was used for pumping and a 640-nm LD was used for probing (Fig. 1). Each beam was collimated through a polarization-maintaining single-mode (SM) fiber and a doublet lens for spatial mode filtering. The combined beams were directed to an objective lens [40X, numerical aperture (NA) = 0.95]. The sample position was raster scanned using a three-axis positioning stage driven by piezo actuators. An iris diaphragm was used to adjust the effective NA of the condenser lens in optimizing the signal-to-noise ratio. An auto-balanced photodetector (Newfocus, Nirvana) was used to cancel the intensity fluctuation of the probe laser, achieving nearly shot noise limited sensitivity. The probe and pump beam intensities were set to frequencies of ω_1 and ω_2, respectively. A beat signal at $|\omega_1-\omega_2|$ was generated by the PT effect in the sample, and a dual-phase lock-in amplifier was used to demodulate the beat signal. In this study, ω_1 and ω_2 were set at 500 kHz and 600 kHz, respectively.

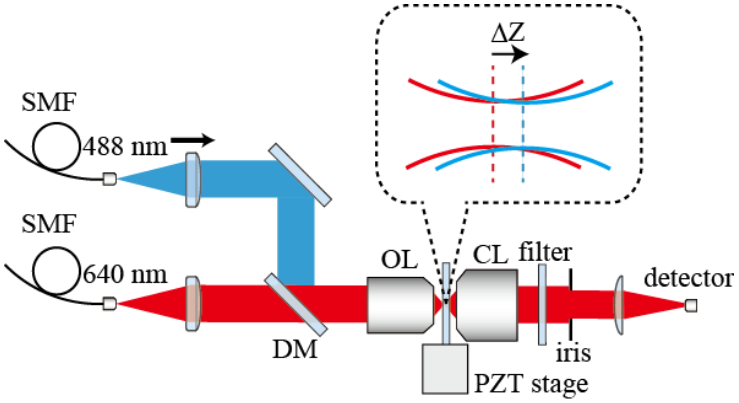

Fig. 1. Schematic illustration of laser diode-based photothermal microscopy. SMF: single mode fiber, DM: dichroic mirror, OBL: objective lens, CL: condenser lens. The distance Δz between the focal planes of the pump and probe beams is controlled by positioning the doublet lens after the SMF in the pump beam path.

3. Results and discussion

To evaluate the usefulness of the present scheme, it is important to understand how the PT signal depends on the beam overlap. For this purpose, the intensity profiles of the pump and probe beams at focus were measured using a knife edge method. A glass slide with chrome-coated lines (Edmond Optics) was mounted on the sample stage and used as a knife edge. A cover slip was attached to the glass slide to avoid spherical aberration, which can be induced by using a dry objective lens. In the knife edge method, the intensity profile is given by the differentiation of the transmitted beam power with respect to the edge position. In our experiment, the differential of the transmitted beam power was directly measured in such a way that the edge positon was modulated in the lateral direction at a frequency of 50Hz with an amplitude of 20 nm. The resulting variation in the transmitted beam power was detected with a lock-in amplifier.

Figure 2(a) shows the intensity profiles of the pump and probe beams in the focal plane. Fitting with a Gaussian provides the full width at half maximum (FWHM) values of the pump and probe beams (282 and 368 nm, respectively). They are only 1.07-1.08 times larger than the diffraction limited spot size (262 and 344 nm, respectively). The displacements between the peak positions of the pump and probe beams in the lateral plane are maintained within ~20 nm. Figure 2(b) shows that the intensity distribution in the axial direction exhibits long tails and fitting with a Lorentzian produces FWHM values of 1.19 and 1.55 μm for the pump and probe beams, respectively.

The spatial offset Δz along the optical axis between the focal planes of the pump and probe beams was controlled by the divergence of the incident pump beam, which was adjusted by positioning the doublet lens after the SM fiber, as depicted in Fig. 1. Figure 2(c) shows the intensity profiles of the pump beam in the axial plane as the position of the doublet

#242711 Received 9 Jun 2015; revised 25 Jul 2015; accepted 25 Jul 2015; published 4 Aug 2015

lens changed. The spatial offset Δz is nearly proportional to the position of the doublet lens [Fig. 2(d)]. The peak intensity depends somewhat on the beam divergence because the incident beam is expanded to overfill the back aperture of the objective lens to maximize the spatial resolution.

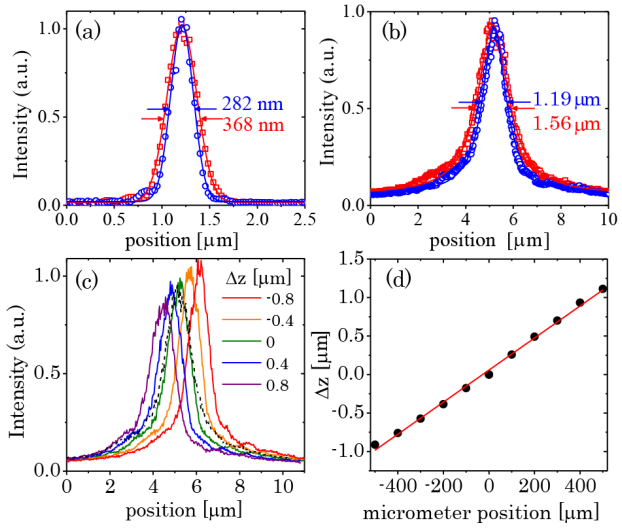

Fig. 2. Intensity profiles of pump (blue) and probe (red) beams in the (a) lateral and (b) axial planes, as measured using a knife edge method. (c) Axial intensity distribution of the pump beam with several offsets of focal plane Δz. The broken line is the intensity profile of the probe beam. (d) Relation between Δz and the position of the doublet lens, which is mounted on a translation stage with a micrometer.

The spatial resolution in PT microscopy is evaluated by changing Δz in the imaging procedure of a single 20-nm gold nanoparticle embedded in polyvinyl alcohol film. The pump and probe beams' power incident on the sample are both 0.2 mW. The time constant of the lock-in amplifier is 0.5 ms and the pixel dwell time is 1 ms.

The PT imaging of individual nanoparticles showed that some particles exhibited twin peaks in the axial direction when Δz was close to zero while others exhibited a single peak, regardless of Δz in the same sample.

Figure 3 shows a typical PT image of a gold nanoparticle that exhibited twin peaks when Δz was close to zero. The amplitude and phase images show that the sign of the probe beam transmissivity (phase of the lock-in amplifier output) changes depending on the axial positon of the sample, and either of the peaks is suppressed with increasing or decreasing Δz [Fig. 3(a)]. This can be explained by the lens-like model, where the probe beam is focused or defocused depending on the sample position and the twin peaks become asymmetric in the presence of the focal plane offset [9–11]. The positive peak (in-phase) is larger than the negative (180° out of phase) peak at Δz = 0 μm.

In the case when the axial intensity profile exhibited a single peak with an offset, the resolution was defined as its FWHM value [Fig. 3(b)]. The axial resolution deteriorated with increasing or decreasing Δz, thus a small |Δz| is preferable for high resolution imaging. However, when Δz was close to zero, the twin peaks emerged, distorting the image of the structured nanomaterials. Hence, it is necessary to suppress the peaks with an appropriate offset. When Δz = −0.4 μm, the intensity profile exhibited a single peak in the axial plane with an FWHM value of 590 nm—smaller than the focal spot size of the pump (probe) beam by 50% (62%). In contrast, the lateral FWHM value at Δz = −0.4 μm was 252 nm [Fig. 3(c)]—smaller than the focal spot size of the pump (probe) beam by 11% (32%). Thus, by providing a small focal plane offset, it was possible to reduce distortion and obtain a high-

#242711 Received 9 Jun 2015; revised 25 Jul 2015; accepted 25 Jul 2015; published 4 Aug 2015

fidelity image with a high spatial resolution. The peak intensity of the PT signal at Δz = –0.4 μm is about 2.1 times larger than that without the offset.

In contrast, some other nanoparticles exhibited single peaks regardless of Δz, as shown in Fig. 4(a). The peak position shifted in the axial direction as Δz changed. The phase images show that the transmissivity of the probe beam was in phase with the pump beam intensity, and the phase value was less affected by Δz. The spatial resolutions in the axial and lateral directions are summarized in Figs. 4(b) and 4(c), respectively. As long as Δz was within 1 μm, the axial and lateral FWHM values were less sensitive to Δz, with averages of 609 and 236 nm, respectively. The lateral FWHM value was close to that of the product of the pump and probe beam intensities (231 nm).

It should be noted that the axial FWHM value was much smaller than that of the product of the pump and probe intensities (890 nm), in Figs. 3 and 4. Furthermore, the intensity of tails in the axial PSF was dramatically reduced, suggesting strong sectioning capability in thick specimens, as the optical sectioning properties resulted from the characteristics of the integrated intensity point spread function.

It is unclear why there were two different types in the same sample. One possible reason is an incomplete thermal lens due to the non-uniformity of the surrounding medium based on local conditions. It is expected that incomplete thermal lens also occurs in imaging biological tissues since they have microscopically non-uninform temperature coefficient of refractive index dn/dT and thermal diffusivity. The results did not depend on the modulation frequencies and pump beam intensity.

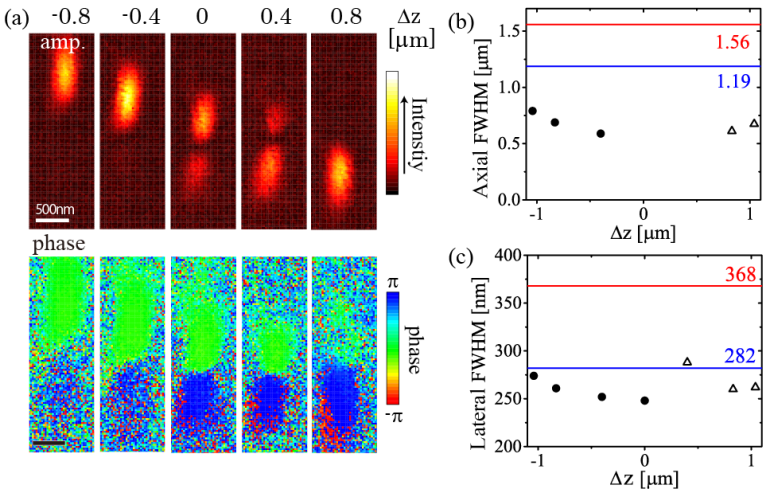

Fig. 3. Photothermal images of a single gold nanoparticle exhibiting twin peaks when the focal offset Δz was close to zero. (a) Intensity distribution in the axial plane with several values of Δz. (b) Axial and (c) lateral FWHM values as a function of Δz. The filled circles and open triangles are the FWHM values for positive (in-phase) and negative (180° out of phase) peaks, respectively.

#242711 Received 9 Jun 2015; revised 25 Jul 2015; accepted 25 Jul 2015; published 4 Aug 2015

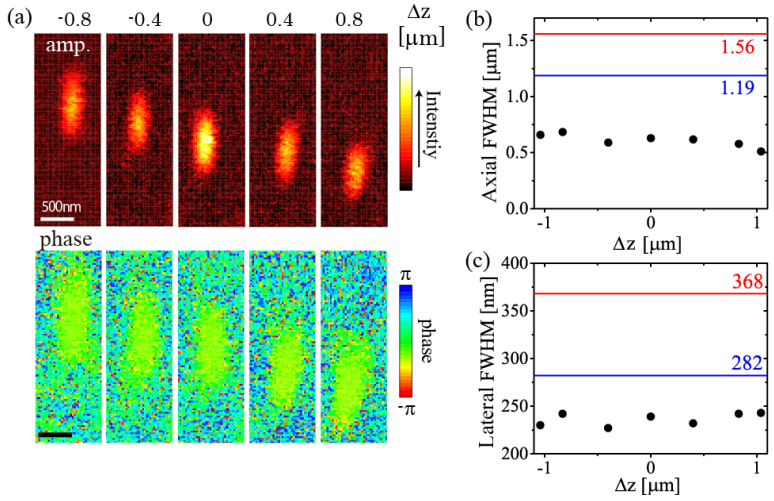

Fig. 4. Photothermal images of a single gold nanoparticle that exhibits a single peak in the axial direction, regardless of the focal plane offset Δz. (a) Intensity distribution in the axial plane with several values of Δz. The upper and lower panels are amplitude and phase images, respectively. The scale bar is 0.5μm. (b) Axial and (c) lateral FWHM values as a function of Δz.

Based on these experimental observations, the procedure for obtaining a PT image with minimized distortion can be summarized as follows. First, it is recommended to measure a sectional image without offset to check for the presence/absence of the distortion. Twin peaks created by the lens-like effect produce a double image and the resulting distortion can be identified from the sign of the signal (or the phase of the lock-in amplifier output). If there are noticeable twin peaks, provide a small offset to suppress either the positive or the negative signal. With decreasing (increasing) Δz, it is possible to enhance the positive (negative) signal while suppressing the negative (positive) signal. Consequently, image distortion is supressed and a high-resolution image can be obtained. A small distortion can be eliminated by simply setting the pixel intensity values to zero. The phase image is useful to check the presence of the distortion due to the dual lobe but the distortion cannot be avoided just by considering the phase.

The 3D imaging of a slice of biological tissue is demonstrated based on this procedure. Figure 5 shows PT images of a slice of a rabbit ovary stained with hematoxylin and eosin (HE). The sample thickness is ~10 μm. Figure 5(a) shows a bright field image of the HE-stained tissues. Both the hematoxylin and eosin molecules were detected in the PT imaging as they absorbed light at a wavelength of 488 nm [5]. The pump and probe beams' power incident on the sample were 0.1 and 0.2 mW, respectively. The focal plane offset was set at Δz = 0 μm. The amplitude and phase images in the lateral [Fig. 5(b)] and axial [Fig. 5(c)] planes show that the positive (in-phase) signal was dominant while the negative (180° out of phase) signal was buried in noise. In this case, it was not necessary to provide an offset. Figure 5(d) and Visualization 1 show 3D images of HE-stained biological tissue. To reconstruct the 3D model, a set of 30 image slices was acquired by changing the sample position in the axial direction with a step size of 0.28 μm. Each image size is 19.6 x 19.6 μm at 200 x 200 pixels. The time constant of the lock-in amplifier was 0.5 ms and the dwell time per point was 1 ms. The complex structures of the cell nucleus and cytoplasm were clearly visualized. One of the advantages of PT imaging is that it dramatically improves the axial resolution over conventional bright field imaging, allowing the production of high-resolution 3D models or high-contrast transverse images for a thick specimen [5].

#242711 Received 9 Jun 2015; revised 25 Jul 2015; accepted 25 Jul 2015; published 4 Aug 2015

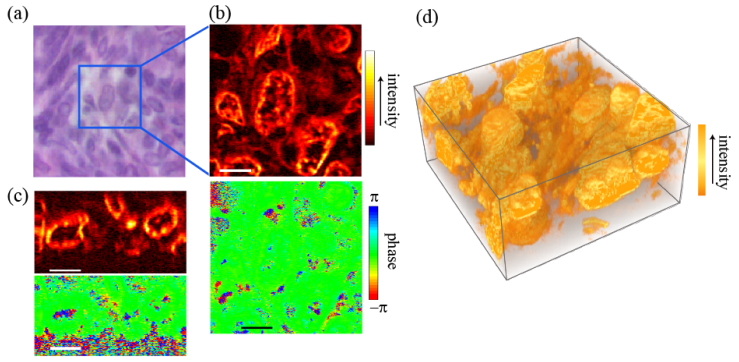

Fig. 5. Photothermal (PT) images of a heamatoxlimai and eosin (HE)-stained tissue. (a) Bright field image of HE-stained tissue. A doublet lens and the same objective lens are used to produce the image on a CMOS camera with a white LED backlight. PT images of the tissue in the (b) lateral and (c) axial planes without focal plane offset. The upper and lower panels indicate amplitude and phase images, respectively. Scale bars are 4 μm. (d) 3D image of HE-stained tissue (see Visualization 1).

In contrast, some of the samples exhibited noticeable distortion in the case of no offset. Figure 6 shows PT images of a slice of mouse melanoma in the lateral plane [Figs. 6(a) and 6(b)] and axial plane [Figs. 6(c) and 6(d)]. Although the positive signal is dominant with Δz = 0 μm, the PT images clearly include large negative signals whose intensity is 20-30% of that of the positive signal [Figs. 6(a) and 6(c)]. This negative signal causes image distortion and can be eliminated by setting the offset at $\Delta z = -0.5$ μm [Figs. 6(b) and 6(d)]. Figure 6(e) and Visualization 2 show the reconstructed 3D image of a slice of mouse melanoma with $\Delta z = -0.5$ μm, in which the 3D distribution of melanin granules is clearly visualized.

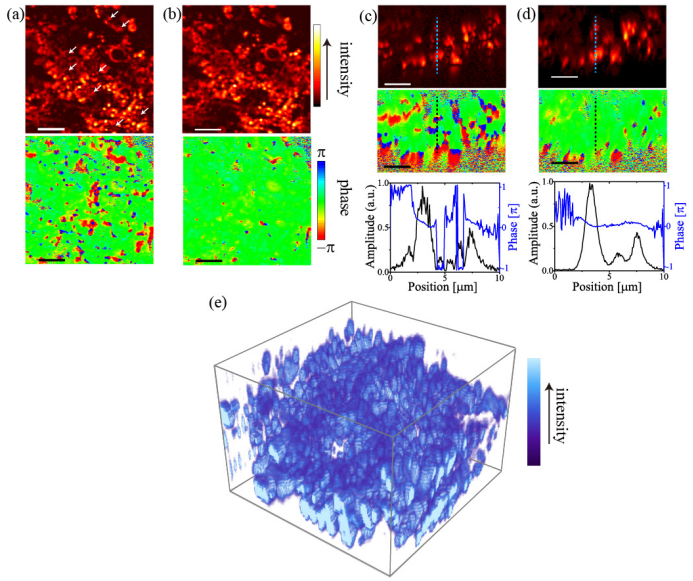

Fig. 6. Photothermal (PT) images of a slice of mouse melanoma in the lateral plane with (a) Δz = 0 μm and (b) $\Delta z = -0.5$ μm. The upper and lower panels indicate amplitude and phase images, respectively. The arrows in (a) indicate a negative (180° out of phase) signal that causes image distortion. The PT images in the axial plane with (c) Δz = 0 μm and (d) $\Delta z = -0.5$ μm. Lower panels show intensity and phase profiles along the broken lines. Scale bars are 4 μm. (e) 3D rendering of a set of 50 image slices (see Visualization 2). Image size is 19.6 x 19.6 x 13.9 μm at 200 x 200 x 50 voxel. The time constant of the lock-in amplifier is 0.5 ms and the dwell time per point is 1 ms.

#242711 Received 9 Jun 2015; revised 25 Jul 2015; accepted 25 Jul 2015; published 4 Aug 2015

In the transmission-mode confocal PT microscopy, the pinhole position should be carefully adjusted so that it lies on a plane one Rayleigh range away from the focal plane [12, 13]. This scheme is useful for measuring a thin specimen. However, because the confocal position is sensitive to the sample thickness, care must be taken with samples of non-uniform thickness or refractive index for the measurement of biological tissues. In contrast, the present scheme was less affected by the non-uniformity of the sample because the confocal pinhole was not used. Furthermore, it can easily be incorporated into the spatially-segmented balanced detection method, which increases the signal-to-noise ratio in PT microscopy [16].

4. Conclusion

We demonstrate a scheme for reducing distortion in photothermal microscopic imaging. Image distortion due to the lens-like effect can be reduced by providing a small focal offset between the pump and probe beams. This scheme does not cause serious degradation in the spatial resolution. When a dry objective lens with an NA of 0.95 was used, the axial and lateral resolution were 0.6 and 0.25 μm in full width at half maximum, respectively, and they were 50% (62%) and 11% (32%) smaller than the focal spot sizes of the pump (probe) beam. Accordingly, the 3D structures of nonfluorescent biological tissues were clearly visualized. Given that the focal offset can be controlled simply by the divergence of the incident beams, this method is easy and simpler than the confocal detection setup, which makes it highly useful in obtaining high-fidelity images with a high spatial resolution.

Acknowledgments

This study was financially supported by a Grant-in-Aid for Scientific Research (No. 15K17735) received from the Japan Society for the Promotion of Science and a joint research project at the Institute of Laser Engineering, Osaka University, under contract number B1-27.